

CasTex: Cascaded Text-to-Texture Synthesis via Explicit Texture Maps and Physically-Based Shading

Mishan Aliev
HSE University
Moscow, Russia

alievmishan78@gmail.com

Dmitry Baranchuk
Yandex Research
Moscow, Russia

dbaranchuk@yandex-team.ru

Kirill Struminsky
Yandex Research, HSE University
Moscow, Russia

kstruminsky@yandex-team.ru

Abstract

This work investigates text-to-texture synthesis using diffusion models to generate physically-based texture maps. We aim to achieve realistic model appearances under varying lighting conditions. A prominent solution for the task is score distillation sampling. It allows recovering a complex texture using gradient guidance given a differentiable rasterization and shading pipeline. However, in practice, the aforementioned solution in conjunction with the widespread latent diffusion models produces severe visual artifacts and requires additional regularization such as implicit texture parameterization. As a more direct alternative, we propose an approach using cascaded diffusion models for texture synthesis (CasTex). In our setup, score distillation sampling yields high-quality textures out-of-the box. In particular, we were able to omit implicit texture parameterization in favor of an explicit parameterization to improve the procedure. In the experiments, we show that our approach significantly outperforms state-of-the-art optimization-based solutions on public texture synthesis benchmarks.

Project page: <https://thecrazymage.github.io/CasTex/>.

1. Introduction

The creation of 3D assets is a central component of modern computer graphics, with demand driven by industries such as film production, industrial design, and computer gaming. High-quality assets should simultaneously meet aesthetic requirements and technical production requirements (e.g., clean mesh topology and limited polygon counts). As a result, 3D modeling remains a labor-intensive creative task that requires multiple expert skills and is difficult to automate due to the scarcity of high-quality data and the challenge of formalizing target criteria.

Meanwhile, the rapid progress of generative models in the visual domain has already transformed many creative domains and is now extending into 3D graphics. Advances

in 3D reconstruction [1, 15, 23] and text-to-image foundation models [30, 31] have enabled early prototypes for fully automated, end-to-end 3D asset generation [18, 21, 27]. These systems leverage the prior knowledge acquired by the diffusion model to generate visually appealing 3D content. However, the resulting assets come in a volumetric representation and are often incompatible with modern graphics engines. Even when volumetric outputs are converted into meshes, the geometry tends to be excessively detailed and may contain high-level structural errors (e.g., multiple faces as in the Janus effect). The limitations mentioned above may be critical when technical requirements must be met.

Texture synthesis offers a more targeted and practical path toward automating parts of the 3D asset pipeline by generating realistic surface appearance for a given shape. In this work, we assume that the geometry is provided by an artist and focus on synthesizing physically based textures [4], which allow for expressive material modeling and realistic rendering under diverse lighting conditions.

Early texture synthesis methods relied on back-projecting synthetic images onto 3D surfaces. However, such approaches are incompatible with PBR materials because RGB images capture only a limited subset of material properties through RGB colors. As an alternative, we consider an optimization-based framework that enables back-propagation through a differentiable renderer to recover full material parameters. In particular, we build on a line of recent work exploring Score Distillation Sampling (SDS) [27] for optimization-based generation.

Our goal is to develop a zero-shot texture-synthesis solution that avoids reliance on auxiliary 3D data and foundation model fine-tuning. However, we observe that the texture synthesis setup unveils the limitations of Score Distillation Sampling applied with modern diffusion models. Consistent with [36], we find that SDS often drives optimization toward images that drift outside the natural image manifold. We expand upon this observation and attribute the effect to inherent properties of latent diffusion models.

Motivated by this analysis, we explore cascaded diffu-

sion models, which operate in RGB space rather than latent space. Our method follows the cascaded-model structure: we first generate a coarse texture using SDS guided by a low-resolution model, then refine it using SDS with a super-resolution model. In the following, we summarize our main contributions.

- We study the limitations of Score Distillation Sampling when applied to latent diffusion models. We show that the corresponding optimization procedure tends to converge to images outside the natural image domain.
- Based on these insights, we introduce CasTex, a texture-synthesis approach using Score Distillation Sampling with cascaded pixel-space diffusion models. The proposed method mimics the architecture of a diffusion model and acts in two stages. The first stage generates a coarse texture, while the second stage improves the overall quality of the texture obtained in the first stage.
- We demonstrate that CasTex outperforms state-of-the-art optimization-based texture synthesis solutions on the Objaverse dataset. Score Distillation Sampling in pixel space allows omitting additional regularizers required in previous works and enables efficient, high-resolution texture generation. Additionally, we report the scaling performance of our method with the diffusion model size, the impact of lighting conditions used during training, and the role of physically-based textures.

2. Related Work

Generating high-quality textures for 3D objects is a longstanding challenge in computer graphics and machine learning. Early approaches are based on category-specific generative models, such as generative adversarial networks (GANs) like Texture Fields [26], SPSG [10], LTG [37], and Texturify [34]. These methods often struggle with limited generalization and required extensive manual adjustments. Recent advances in large-scale text-to-image diffusion models [30, 31] have transformed texture synthesis, allowing more flexible and realistic results. However, different approaches vary in how they leverage diffusion models to incorporate 3D information and ensure texture consistency.

Diffusion-based texture generation. A significant part of recent works formulates texture generation as an iterative inpainting process using depth-conditioned diffusion models. Text2Tex [6], TEXTure [29], and Paint3D [38] generate textures by synthesizing single-view images and progressively refining the texture using different object views. Although these zero-shot approaches allow for training-free generation, they often struggle with seams at visibility boundaries and suffer from baked-in lightning artifacts, leading to global inconsistencies. To mitigate these issues, some methods introduce additional refinement steps: Text2Tex employs an inpainting diffusion model for post-

processing, while Paint3D refines textures directly in UV space. TexDreamer [20] follows a different approach by directly generating a UV texture map using a fine-tuned diffusion model, avoiding the need for iterative view synthesis and improving consistency across the surface.

An alternative strategy to address inconsistency is to introduce additional structures to enforce coherence between views. SyncMVD [19] tackles this by generating each view independently while employing a synchronization module that aligns outputs in every denoising step of the diffusion model. Similarly, TexFusion [5] suggest a module that aggregates multiview object predictions into a unified latent texture representation, iteratively refining it throughout the diffusion process to ensure consistency across the object.

Another approach, inspired by MVDream [32], leverages consistent multiview image generation as an initialization step for texture synthesis. Meta 3D TextureGen [2] follows this idea by generating four consistent views, which are projected onto a 3D surface to form an initial texture for subsequent refinement in UV space. MVPaint [8] extends this pipeline by introducing a spatially-aware 3D inpainting stage between projection and UV refinement, further enhancing coherence across different object views.

Optimization-based methods. Optimization-based techniques refine a texture by optimizing an objective function that evaluates rendered views. Early approaches such as CLIP-Mesh [24] and Text2Mesh [22] use differentiable rendering with CLIP [28] as a guidance signal to iteratively update texture parameters. While these methods are simple and training-free, they tend to produce blurred textures lacking high-frequency detail.

More recent work incorporate diffusion models to improve texture optimization. Latent-Paint [21], Fantasia3D [7], and Paint-it [36] combine differentiable rendering with Score Distillation Sampling (SDS) technique [27], distilling knowledge from a diffusion model to refine textures. Although this approach enhances realism, it often suffers from color oversaturation and high-frequency artifacts. FlashTex [12] mitigates some of these issues by using a fine-tuned multiview model to generate an initial textured view of the object, followed by an optimization stage using L2-loss and SDS for refinement.

In this work, we continue the line of work employing SDS. However, we attribute some of the artifacts to the underlying latent diffusion model and propose using a pixel space model. Aiming at physically plausible textures, we use a text-to-image model pretrained on natural images and resort from using synthetic data for multiview model adaptation.

PBR texture generation. Most of the works discussed above generate only RGB, limiting physical realism. Fantasia3D [7], Paint-it [36], and FlashTex [12] propose to synthesize more advanced physically based textures [4], which

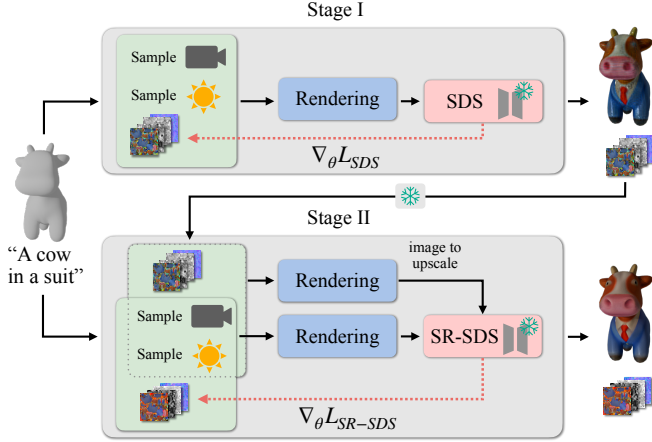


Figure 1. Overall pipeline. Our method consists of two stages. In the first stage, given a 3D mesh and a text prompt, we use a differentiable rendering pipeline to generate random views of the model under varying lighting conditions. The texture, initialized randomly, is optimized using the SDS gradient $\nabla_{\theta} \mathcal{L}_{SDS}(\theta)$ (Eq. 1). In the second stage, we refine the texture produced in stage one using SDS with a super-resolution diffusion model. For each camera view and lighting setup, we render two images: one using the fixed texture from the first stage, and one using the current texture being optimized. We denote the SDS gradient adapted to the super-resolution model as $\nabla_{\theta} \mathcal{L}_{SR-SDS}$. Using the former image as a conditioning input, we backpropagate the SR-SDS gradients through the latter image.

are able to mimic different materials and look realistic under different lighting. We pursue a similar goal but employ a different class of generative models and demonstrate the advantages of SDS in pixel space.

3. Method

We leverage a pretrained text-to-image diffusion model to synthesize high-quality textures. Because such models are trained for unconditional image generation rather than texture optimization, we employ Score Distillation Sampling (SDS) to obtain gradients compatible with our differentiable rendering pipeline. Specifically, we couple SDS with a cascaded diffusion model to refine textures across multiple resolutions. The overall architecture is illustrated in Figure 1.

3.1. Preliminaries on Score Distillation Sampling for Gradient Based Generation

SDS defines gradients used to update the parameter $\theta \in \Theta$. Let $x_0 = g(\theta, c)$ denote the mapping from the parameter θ and a random variable c to a rendered image x_0 . Given a diffusion process in which noise images are generated as $x_t = \sqrt{\bar{\alpha}_t}x_0 + \sqrt{1 - \bar{\alpha}_t}\epsilon$ at timestep t with noise scale $\bar{\alpha}_t$, the method leverages a pretrained diffusion model $\epsilon_{\phi}(x_t; y, t)$ to define a pseudo-objective that guides updates

to x_0 .¹ The pseudo-objective $\hat{x}_0^t = \frac{x_t - \sqrt{1 - \bar{\alpha}_t}\epsilon_{\phi}(x_t, t, y)}{\sqrt{\bar{\alpha}_t}}$ provides a single-step estimate of the clean image x_0 from the noisy sample x_t using the diffusion model’s prediction.

The resulting gradient is estimated as

$$\nabla_{\theta} \mathcal{L}_{SDS}(\theta) = \mathbb{E}_{t, \epsilon, c} \left[w(t)(x_0 - \hat{x}_0^t) \frac{\partial x_0(\theta, c)}{\partial \theta} \right], \quad (1)$$

where $w(t)$ is a scalar weight parameter. While [27] express SDS in terms of noise prediction ϵ , we present an equivalent formulation in the x_0 -domain. Viewed from one perspective, this gradient has the form of a mean-squared-error objective, $\mathbb{E} [w(t) \|x_0 - \hat{x}_0^t\|^2]$, where the dependence of \hat{x}_0^t on θ is ignored when computing the gradient. From another perspective, the analysis in [27] shows that SDS minimizes the divergence $\mathcal{L}_{SDS}(\theta) = \mathbb{E}_{t, c} \text{KL}(q(x_t | t) \| p_{\phi}(x_t | y, t))$ where the pretrained diffusion model provides the score $\epsilon_{\phi}(x_t; y, t) = \nabla_{x_t} \log p_{\phi}(x_t | y, t)$.

Originally, SDS was applied to pixel-space diffusion models that generate low-resolution images. However, pretrained pixel-space models are relatively rare, and consequently most applications of SDS have focused on latent diffusion models (LDMs). These models approximate the distribution of low-dimensional latent embeddings of high-resolution images rather than the images themselves. Importantly, the encoder mapping $\text{enc}(\cdot)$ that produces these embeddings is differentiable and can therefore be incorporated directly into the image-generation pipeline:

$$g_{\text{latent}}(\theta, c) = \text{enc}(g_{\text{pixel}}(\theta, c)). \quad (2)$$

A key advantage of LDMs is their ability to guide the synthesis of high-resolution images more efficiently than pixel-space models. However, this comes at the cost of additional computation due to the encoder’s forward and backward passes. In Section 4, we further examine the implications of applying SDS in latent space rather than pixel space.

3.2. Applying SDS with Super-Resolution Diffusion Models

The main drawback of pixel-space diffusion models is that generating high-resolution images demands substantial computational resources. While latent diffusion models mitigate this cost by using a VAE [16] to encode images into a lower-dimensional latent space, pixel-space approaches typically rely on a cascaded generation process. In such pipelines, a diffusion model first produces a low-resolution image, and a subsequent super-resolution model upsamples it to the target resolution.

In [27], the authors apply SDS only with a low-resolution diffusion model. However, because this model is trained on

¹Throughout the paper, we assume that the diffusion model ϵ_{ϕ} incorporates the conditioning y via classifier-free guidance.

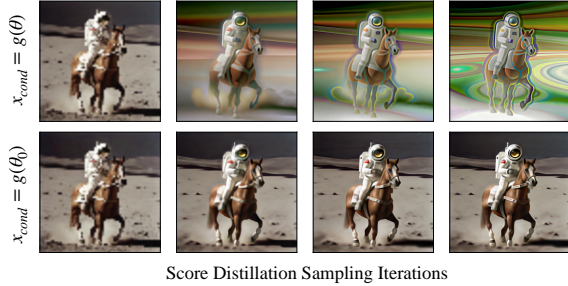


Figure 2. Score distillation sampling applied to a super-resolution diffusion model. The horizontal axis indicates optimization progress over time. *Top row*: the same image $g(\theta)$ is used both as a diffusion-model input x and as the conditioning image x_{cond} for super-resolution. This setup is unstable and causes the optimization to drift away from the original image. *Bottom row*: the same procedure, but with fixed super-resolution condition $x_{cond} = g(\theta_0)$. The fixed condition anchors the optimization dynamics, preserving the structure of the initial image.

downsampled images, it often fails to recover fine-grained details and high-frequency texture. To achieve high-fidelity outputs, we adopt the architectural structure of cascaded diffusion models. Specifically, we first run SDS with a low-resolution diffusion model, and then refine the output using SDS in combination with a super-resolution model. In the text-to-image setting, the second-stage model takes as input a low-resolution image along with a text prompt and timestep. This setup naturally suggests two strategies for applying SDS during refinement. The first strategy is to use the rendered image $g(\theta, c)$ as the diffusion-model input in SDS, while providing a downsampled version of the same image as a conditioning signal. Intuitively, this approach iteratively enriches the texture by adding details that were missing in previous gradient steps. The second strategy is to freeze the parameters $\theta_0 = \theta$ obtained from the first stage, then run SDS with a fresh copy of θ as the optimization target and treat θ_0 as a fixed conditioning input. In this case, the first-stage result serves as an anchor that guides the gradient descent dynamics.

In our experiments, the first strategy tends to be less stable and often drifts toward out-of-domain images, whereas the second strategy more reliably enhances resolution while preserving the details of the initial result. Figure 2 illustrates these observations.

3.3. Differentiable Physically Based Shading

Our texture synthesis approach applies SDS in a setting, where $g(\theta, z)$ renders an image of a fixed 3D model given a set of texture parameters θ and a random camera position and scene lighting specified by z . Rendering follows the differentiable rasterization pipeline of [25] implemented using Nvdiffrast [17].

Our textures follow the Disney physically based material model [4] with $\theta = (\theta_d, \theta_r, \theta_m, \theta_n)$ representing diffuse albedo, specular roughness, metalness, and a normal map, respectively. This parameterization ensures compatibility with standard real-time rendering engines. Lighting is provided via an environment map using a split-sum approximation of the outgoing radiance integral [14].

4. Score Distillation Sampling Analysis

In this section, we analyze Score Distillation Sampling (SDS) to motivate our proposed method. We argue that SDS applied to latent diffusion models is inherently prone to generating artifacts due to the ill-posed nature of the underlying optimization problem.

Following common practice, we conduct the analysis in the simplified setting of image generation. We use a mapping $g_{id}(\theta, c) = \theta$ that produces a 2D image θ and while ignoring the stochastic variable. The goal is to recover images that are consistent with the diffusion model’s distribution using gradient descent. Intuitively, SDS gradients are expected to push generated images $g(\theta, c)$ toward the manifold of natural images. Using the chain rule, these gradients also propagate to the parameter θ . However, with latent diffusion models, guidance occurs in latent space: $g(\theta, c) = \text{enc}(g_{id}(\theta, c))$. As a result, the training signal must propagate through the encoder, placing additional constraints on the optimization trajectory.

To isolate the behavior of SDS and exclude confounding factors such as model mis-specification or stochastic gradient noise, we consider a toy diffusion model that represents a degenerate distribution $\delta(x - x^*)$ concentrated at a single image x^* . This setup removes issues arising from imperfect score estimation or excessive variance in Eq. 1. For the degenerate distribution, the optimal score model reduces to a closed-form denoiser:

$$\epsilon_{degenerate}(x_t) = \frac{x_t - \sqrt{\alpha_t}x^*}{\sqrt{1 - \alpha_t}}. \quad (3)$$

With constant weights $w(t) = 1$, the SDS gradient simplifies to the deterministic gradient of the mean squared error:

$$\nabla_{\theta} \mathcal{L}_{SDS}(\theta) = \nabla_{\theta} \|g(\theta) - x^*\|^2. \quad (4)$$

Thus, in this idealized setting we can write

$$\mathcal{L}_{SDS}(\theta) = \|g(\theta) - x^*\|^2 \quad (5)$$

We optimize Eq. 5 under various parameterizations and report the results in Figure 3. For pixel-space diffusion, where $g(\theta) = \theta$, gradient descent quickly converges to $\theta \approx x^*$ (*top row, left*). For latent-space model, we assume x^* to be the latent code of the same image and minimize $\|\text{enc}(g(\theta)) - x^*\|^2$. Although the gradient descent converges and the decoder maps $\text{enc}(\theta)$ to the original image

(*top row, right*), the optimized parameter θ itself is a poor approximation to the original image (*top row, middle*). In other words, SDS with latent diffusion models frequently finds near-optimal latent solutions whose pre-images fall outside the natural image domain.

This phenomenon does not significantly affect some text-to-3D tasks, where the optimization variable is not directly visualized. However, in the context of texture synthesis—where θ is the texture—these artifacts severely limit the applicability of SDS.

To address this issue, [36] proposes parameterizing textures via a deep convolutional network, following the Deep Image Prior (DIP) framework [35]. This parameterization acts as an implicit regularizer that discourages unnatural images. Although effective to some extent, it introduces an additional convolutional network into the pipeline and, as we show below, still leaves noticeable artifacts.

The bottom row of Figure 3 illustrates SDS optimization with the DIP parameterization. Let the generated image be produced by a U-Net with parameters θ_{dip} and a fixed Gaussian noise input. We denote this differentiable generator as $g_{UNet}(\theta_{dip})$. We optimize Eq. 5 under both pixel-space and latent-space models. The DIP parameterization substantially improves the solution for latent diffusion (*middle row*), reducing the artifacts seen with the explicit parameterization. However, even with DIP, SDS in latent space fails to match the reconstruction quality of directly optimizing the latent code (*middle and right bottom row*).

We also experimented with additional regularization based on decoder outputs but observed no meaningful improvement over standard SDS. In contrast, pixel-space optimization achieves significantly better reconstruction in both explicit and implicit parameterizations.

5. Experiments

We evaluated our method on the Objaverse dataset [11], comparing it both qualitatively and quantitatively with state-of-the-art texture synthesis approaches. We also performed an ablation study to validate key design decisions.

5.1. Evaluation setup

For our method, we took DeepFloyd-IF [33] as an open-source cascaded diffusion model. We considered the XL (64×64) and L (256×256) models for the first and second stages, respectively. Also, we considered the setting with the smaller model IF(M) at the first stage to explore the effect of the diffusion model scale on the texture quality.

We compared the proposed method with four baselines that represent various approaches to texture synthesis. First, Text2Tex [6] is a well-established backprojection-based method generating non-PBR textures. Second, SyncMVD [19] is a recent method that enforces consistency by generating and synchronizing multiple views. Third,

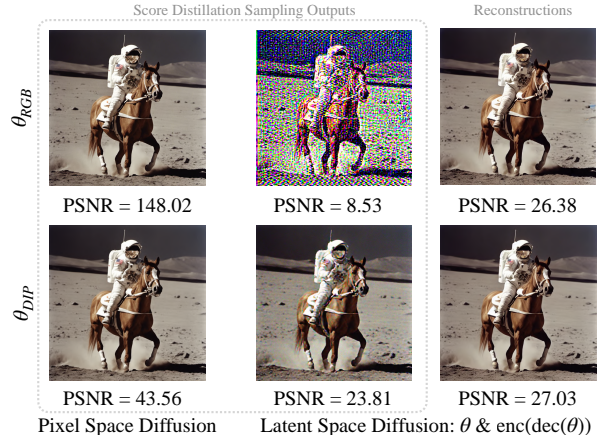


Figure 3. Optimization based image generation for a toy single-mode diffusion model. We study the effect of image parameterization and the difference between pixel and latent-space diffusion models. Score Distillation Sampling (SDS) finds the distribution mode for both latent-and pixel-space diffusion models. *Top row*: the pixel space model achieves near-perfect reconstruction quality measured by PSNR. The latent code $\text{enc}(\theta_{RGB})$ is also close to the mode and leads to high quality reconstruction. However, for the latent model the optimized parameter θ_{RGB} fails to approximate the original image. *Bottom row*: The implicit regularization proposed in [36] significantly improves the results for SDS for the latent diffusion model, but still falls short of the image reconstruction given by the decoder or pixel space diffusion model.

Paint-it [36] is a simplistic optimization-based method using SDS. The crucial distinction between our method and Paint-it is the underlying diffusion model and texture parameterization. Finally, FlashTex [12] is another recent approach using SDS. It addresses the limitations of previous methods by fine-tuning the model used for guidance on multiview 3D data with controlled lighting. Again, all of the baselines are based on latent diffusion models for texture synthesis.

To evaluate the quality of generated textures, we computed the Fréchet Inception Distance (FID) [13] and Kernel Inception Distance (KID) [3] metrics on a subset of the Objaverse dataset [11]. Specifically, we adopted the same curated subset used in Text2Tex [6], which includes 410 high-quality textured meshes from 225 distinct categories. This subset was originally filtered to exclude meshes with simplistic or inconsistent textures, category mismatches, and over-triangulated or scanned objects. All methods generated textures for the same set of untextured 3D meshes using identical text prompts, then each textured mesh is rendered from 20 fixed viewpoints at a resolution of 512×512 with a white background using Blender [9]. We provide a detailed evaluation setup in Appendix A, where we specify the most critical rendering parameters (e.g., lighting configuration, render engine, etc.) to ensure accurate comparisons.

Method	Size (↓)	FID (↓)	KID ($\times 10^{-3}$, ↓)	Runtime (seconds, ↓)
Non-SDS methods				
Text2Tex	2.5B	21.3	3.9	549
SyncMVD	1.5B	20.3	2.7	55
SDS methods				
Paint-It	1B	25.2	6.7	892
FlashTex	1.3B	29.0	9.5	280
CasTex (M)	400M	24.6	5.4	38
CasTex (M+L)	1.6B	22.9	4.6	628
CasTex (XL)	4.3B	22.4	4.2	174
CasTex (XL+L)	5.5B	19.5	3.0	710

Table 1. Comparison of FID and KID scores for different text-to-texture generation methods. Notably, even with the smallest diffusion model, our method outperforms optimization-based baselines. As expected, the super-resolution stage improves the results for both stages. Surprisingly, in our evaluation, the older back-projection-based method outperforms the optimization-based method and is only rivaled by our largest setup. We use NVIDIA A100 80GB for time measurements and generate textures with a resolution of 1024x1024 pixels.

5.2. Main Results

Automated quality assessment. We report FID and KID scores in Table 1. Our smallest single-stage setup outperformed the two optimization-based approaches. The two-stage cascaded diffusion approach achieved the best performance, outperforming all baselines. We illustrate the two stages contrasting with the noisy results from latent diffusion and provide additional illustrations in Appendix C. The second stage significantly refines the textures, enhancing fine-grained details and coherence.

Notably, the weak performance of FlashTex on the benchmark is the result of the limited generalization abilities of the Light ControlNet proposed by the authors. To our surprise, Text2Tex delivered competitive results. Even though the method is the oldest baseline, the back-projected photo-realistic images lead to photo-realistic renders. SyncMVD also achieved strong scores, outperforming other baselines, which highlights the effectiveness of its multi-view synchronization approach.

Our method also achieves competitive synthesis times, with the two-stage variant completing generation in 12 minutes per mesh – comparable to baselines while delivering better quality. For time-constraint applications, the single-stage variant generates plausible textures in just 3 minutes, offering a compelling trade-off between computational efficiency and texture realism, making it suitable for time-constraint applications.

User preference study. In addition, we conduct a human study to compare the perceptual quality of our generated textures with the baseline methods. The evaluation is con-

Method	FID (↓)	KID ($\times 10^{-3}$, ↓)
CasTex (diffuse map only)	21.2	3.7
CasTex	19.5	2.4

Table 2. Ablation of Physically Based Rendering (PBR) components. Optimizing the full set of PBR components improves texture quality compared to synthesizing only the diffuse map.

ducted by professional assessors, asked to make a decision between two rendered textures given a textual prompt. The decision is made according to the texture quality and textual alignment. For each pair, three responses are collected and the final result is determined by majority vote. For evaluation, we use 256 random objects from the previously mentioned Objaverse subset.

As shown in Figure 5, our large two-stage approach outperforms all the baselines. Figure 4 presents a qualitative comparison of our method with the four baselines. The comparison against the first stage confirms that the second stage is highly effective for further texture refinement.

In addition, we provide the results of our method using the smaller version of DeepFloyd-IF that contains 400M parameters. We observe that our method still outperforms most competing works.

Overall, our method achieves impressive quality, effectively producing detailed, seamless, and high-fidelity textures, as further confirmed by quantitative results.

5.3. Ablation study

We conducted a series of experiments to understand the role of key design choices in our approach.

Do the PBR components improve textures? PBR components enable the modeling of complex visual effects like reflections and material properties, avoiding baked-in lighting and improving realism, as qualitatively demonstrated in Figure 6 (additional illustrations in Appendix E).

We compare our full PBR-based approach with a baseline that generates only the diffuse map, one of the PBR components. As shown in Table 2, generating the full set of PBR maps leads to better FID and KID scores compared to generating the diffuse map alone. Despite better metrics, a closer study of illustrations indicates that the method occasionally struggles with baked-in lighting.

Can our second stage improve other methods? We hypothesize that our second stage in the PBR texture generation pipeline can improve the results of other texture synthesis methods. To validate this, we experiment with applying our second stage to well-initialized diffuse maps from another method.

As shown in Table 3, our second stage can effectively generate PBR textures when initialized with diffuse maps

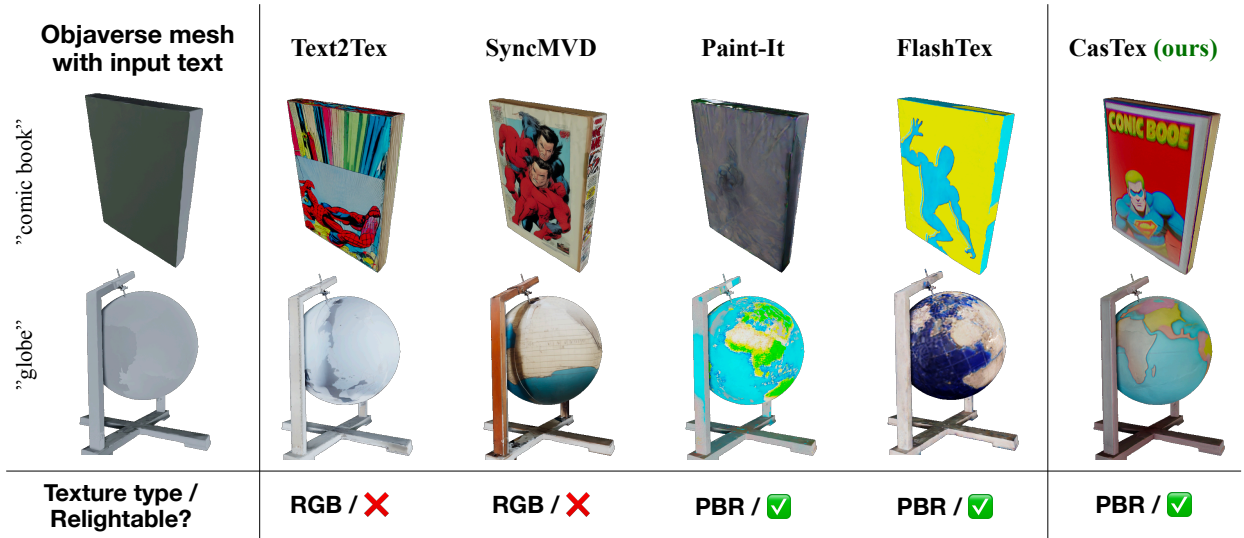


Figure 4. Qualitative comparison. We synthesized textures for models from the Objaverse dataset using the proposed approach and several recent competing methods. Our method generates seamless textures with softer colors compared with latent diffusion-based approaches.

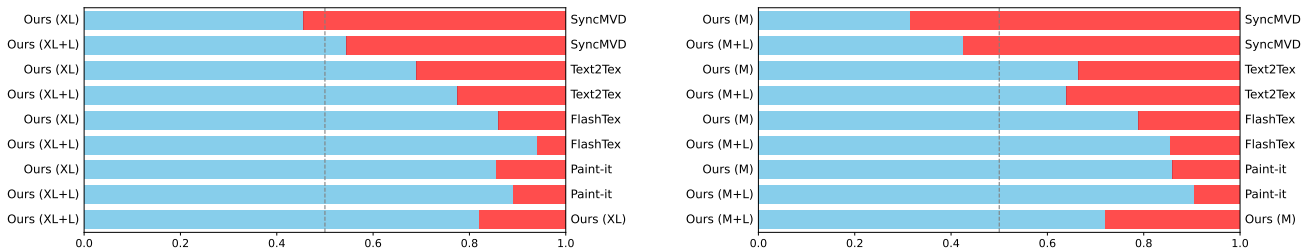


Figure 5. Human preference study comparing our method with competing optimization based and back-projection baselines.

Method	FID (↓)	KID ($\times 10^{-3}$, ↓)
Text2Tex	21.3	3.9
CasTex (Text2Tex init, k_d frozen)	20.9	3.7
CasTex (Text2Tex init, k_d trained)	19.7	3.6

Table 3. Ablation study of initializing our second stage with Text2Tex outputs to generate PBR textures. The results show that allowing the diffuse map (k_d) to be optimized during our second stage leads to significant improvements in both FID and KID metrics, while keeping the diffuse map frozen maintains the same FID but slightly increases KID. This suggests that our approach can effectively serve as an enhancement module for existing texture generation methods.

from Text2Tex. We explore two configurations: (1) keeping the initial diffuse map fixed (k_d frozen) and (2) fine-tuning the diffuse map during PBR generation (k_d trained).

The results show that even when the diffuse map is kept frozen, our approach improves both FID and KID scores

over the original Text2Tex output. This improvement is likely limited because freezing k_d also preserves any baked-in lighting information present in the initial diffuse map, preventing our method from correcting these inconsistencies. In contrast, when we allow diffuse map optimization (k_d trained), our approach achieves a significant improvement in FID and a further, albeit smaller, improvement in KID. This shows that enabling diffuse map refinement helps to correct lighting artifacts and better harmonize the entire PBR material set, highlighting its potential as a versatile enhancement module for various texture generation pipelines.

How does environment lighting affect results? Among recent works, Paint-it is the most similar to ours, as it also relies solely on SDS-based optimization. Unlike our approach, their rendering algorithm uses a brighter, uniform lighting environment map for training, which can make it difficult to distinguish between specular and rough diffuse surfaces. Instead, we propose an environmental map with a single pronounced light source, a weaker ambient lighting component, and additional augmentations with horizontal rotations. For final evaluation, we also employ a distinct

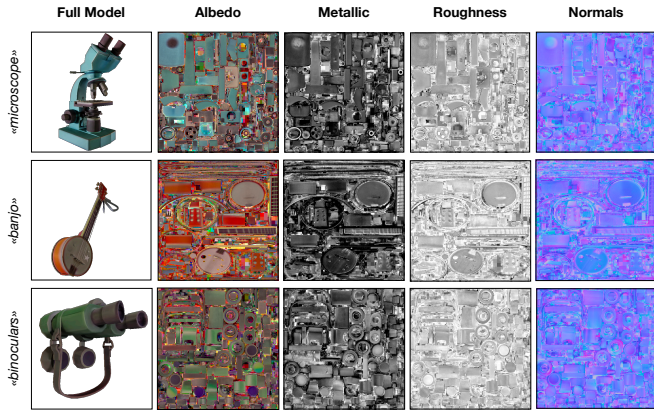


Figure 6. Qualitative analysis of PBR components generated by CasTex. Lighter colors indicate higher metallic and roughness values for the corresponding texture components. The microscope shows a clear separation between painted non-metals and polished steel optics, with low roughness for the lenses and higher values for rubber and plastics. The banjo treats the wooden shell and drumhead as non-metal while assigning metalness to the hardware and a semi-gloss roughness to the lacquered wood. The binoculars further demonstrate semantic consistency by distinguishing matte rubber eyecups and strap from the painted housing and metallic fasteners. Across all three, the normal map contributes fine surface detail without altering the geometry.

Method (Training envlight)	Studio light eval		Paint-It light eval	
	FID (↓)	KID ($\times 10^{-3}$, ↓)	FID (↓)	KID ($\times 10^{-3}$, ↓)
Paint-It (Paint-It)	25.2	6.7	26.8	6.2
CasTex (Paint-It)	22.2	4.6	24.7	4.5
Paint-It (Proposed)	24.5	6.4	26.9	6.6
CasTex (Proposed)	19.5	2.4	24.1	4.4

Table 4. Ablation of environment lighting. We investigate how different training and evaluation environment maps affect PBR texture quality. Both CasTex and Paint-It are trained on either the Paint-It or our Proposed maps. Performance is then evaluated under two distinct lighting conditions: our proposed Studio (which differs from both training maps) and the Paint-It maps. Our full pipeline (CasTex trained with the Proposed envlight) achieves the best results in both evaluation scenarios. Notably, CasTex also outperforms Paint-It even when both are trained and evaluated on the less expressive Paint-It map.

studio lighting environment, different from the one used for training (for more details, see Appendix A).

To disentangle the effects of the model from the lighting strategy, we evaluated all combinations of training and evaluation setups against Paint-It in Table 4. Our full pipeline (CasTex with our proposed envlight) consistently achieves the best metrics across both evaluation scenarios, demon-

Res.	Method	Runtime (min, ↓)	VRAM (GB, ↓)	FID (↓)	KID ($\times 10^{-3}$, ↓)
1K	CasTex (DIP)	≈ 14	20.7	20.8	3.7
	CasTex	≈ 12	10.5	19.5	2.4
2K	CasTex (DIP)	≈ 24	52.3	21.1	3.9
	CasTex	≈ 12	10.8	19.7	2.6
4K	CasTex (DIP)	OOM	OOM	–	–
	CasTex	≈ 12	12	19.6	2.6

Table 5. Ablation study on DIP and scalability. We compare our explicit method against its own DIP-based variant. At 1K, DIP offers no quality benefits while being slower. At higher resolutions, it scales poorly and fails at 4K, whereas our method maintains nearly constant runtime and VRAM usage. We use the same NVIDIA A100 80GB for all experiments; OOM = out of memory, 1K=1024 \times 1024, 2K=2048 \times 2048, 4K=4096 \times 4096.

strating its robust performance. Even when both models are trained and evaluated on the same, less expressive Paint-It environment map, CasTex outperforms Paint-It, highlighting an advantage of our model that stems from its design.

DIP versus explicit parameterization. Following the approach of our closest competitor, Paint-it, we integrate Deep Image Prior (DIP) [35] into our method and evaluate its impact on texture optimization (see Section 4 for details). We test our base model CasTex (XL+L) against its modification with implicit texture representation, CasTex (DIP, XL+L). Table 5 shows the results for quality, performance, and scalability across multiple resolutions.

The analysis reveals two key findings. First, the DIP-based variant does not provide a significant quality benefit while being noticeably slower at all resolutions. Second, our method with explicit parameterization demonstrates remarkable scalability, maintaining a nearly constant runtime and only marginal VRAM growth. This confirms that for our cascaded approach, the added complexity of DIP is unnecessary for quality and scalability, making our explicit parameterization the best choice for practical applications.

6. Conclusion

In this work, we introduced CasTex, an optimization-based texture synthesis method that leverages cascaded pixel-space diffusion models with explicit texture parameterization. We motivated our design through an analysis highlighting the limitations of latent diffusion models. Our method demonstrates improved performance over recent optimization-based texture synthesis approaches, as measured by automated metrics and user studies. While CasTex benefits from physically-based textures, we still observe baked-in lighting and occasional inconsistencies between textures and the underlying geometry. Future work may address baked-in lighting artifacts or the aforementioned SDS limitations in latent-space models.

Acknowledgements

The paper was prepared within the framework of the HSE University Basic Research Program and was supported in part through computational resources of HPC facilities at HSE University. This research was also supported by Yandex Education.

We would like to thank Roman Chulkevich and Viacheslav Kozyrev for their assistance with the computing cluster. We also thank Ksenia Ushatskaya for her help with the visualization of the generated textures used in the paper teaser. Special thanks go to Maxim Kodryan, whose mere existence made this research journey considerably more enjoyable.

References

- [1] Jonathan T Barron, Ben Mildenhall, Dor Verbin, Pratul P Srinivasan, and Peter Hedman. Zip-nerf: Anti-aliased grid-based neural radiance fields. In *Proceedings of the IEEE/CVF International Conference on Computer Vision*, pages 19697–19705, 2023. 1
- [2] Raphael Bensadoun, Yanir Kleiman, Idan Azuri, Omri Harosh, Andrea Vedaldi, Natalia Neverova, and Oran Gafni. Meta 3d texturegen: Fast and consistent texture generation for 3d objects. *arXiv preprint arXiv:2407.02430*, 2024. 2
- [3] Mikołaj Bińkowski, Danica J Sutherland, Michael Arbel, and Arthur Gretton. Demystifying mmd gans. *arXiv preprint arXiv:1801.01401*, 2018. 5
- [4] Brent Burley and Walt Disney Animation Studios. Physically-based shading at disney. In *Acm Siggraph*, pages 1–7. vol. 2012, 2012. 1, 2, 4
- [5] Tianshi Cao, Karsten Kreis, Sanja Fidler, Nicholas Sharp, and Kangxue Yin. Textfusion: Synthesizing 3d textures with text-guided image diffusion models. In *Proceedings of the IEEE/CVF International Conference on Computer Vision*, pages 4169–4181, 2023. 2
- [6] Dave Zhenyu Chen, Yawar Siddiqui, Hsin-Ying Lee, Sergey Tulyakov, and Matthias Nießner. Text2tex: Text-driven texture synthesis via diffusion models. In *Proceedings of the IEEE/CVF International Conference on Computer Vision*, pages 18558–18568, 2023. 2, 5
- [7] Rui Chen, Yongwei Chen, Ningxin Jiao, and Kui Jia. Fantasia3d: Disentangling geometry and appearance for high-quality text-to-3d content creation. In *Proceedings of the IEEE/CVF international conference on computer vision*, pages 22246–22256, 2023. 2
- [8] Wei Cheng, Juncheng Mu, Xianfang Zeng, Xin Chen, Anqi Pang, Chi Zhang, Zhibin Wang, Bin Fu, Gang Yu, Ziwei Liu, et al. Mvpaint: Synchronized multi-view diffusion for painting anything 3d. *arXiv preprint arXiv:2411.02336*, 2024. 2
- [9] Blender Online Community. *Blender - a 3D modelling and rendering package*. Blender Foundation, Stichting Blender Foundation, Amsterdam, 2018. 5
- [10] Angela Dai, Yawar Siddiqui, Justus Thies, Julien Valentin, and Matthias Nießner. Spsg: Self-supervised photometric scene generation from rgb-d scans. In *Proceedings of the IEEE/CVF Conference on Computer Vision and Pattern Recognition*, pages 1747–1756, 2021. 2
- [11] Matt Deitke, Dustin Schwenk, Jordi Salvador, Luca Weihs, Oscar Michel, Eli VanderBilt, Ludwig Schmidt, Kiana Ehsani, Aniruddha Kembhavi, and Ali Farhadi. Objaverse: A universe of annotated 3d objects. In *Proceedings of the IEEE/CVF Conference on Computer Vision and Pattern Recognition*, pages 13142–13153, 2023. 5, 12
- [12] Kangle Deng, Timothy Omernick, Alexander Weiss, Deva Ramanan, Jun-Yan Zhu, Tinghui Zhou, and Maneesh Agrawala. Flashtex: Fast relightable mesh texturing with lightcontrolnet. In *European Conference on Computer Vision*, pages 90–107. Springer, 2024. 2, 5
- [13] Martin Heusel, Hubert Ramsauer, Thomas Unterthiner, Bernhard Nessler, and Sepp Hochreiter. Gans trained by a two time-scale update rule converge to a local nash equilibrium. *Advances in neural information processing systems*, 30, 2017. 5
- [14] Brian Karis and Epic Games. Real shading in unreal engine 4. *Proc. Physically Based Shading Theory Practice*, 4(3):1, 2013. 4
- [15] Bernhard Kerbl, Georgios Kopanas, Thomas Leimkühler, and George Drettakis. 3d gaussian splatting for real-time radiance field rendering. *ACM Trans. Graph.*, 42(4):139–1, 2023. 1
- [16] Diederik P. Kingma and Max Welling. Auto-Encoding Variational Bayes. In *2nd International Conference on Learning Representations, ICLR 2014, Banff, AB, Canada, April 14-16, 2014, Conference Track Proceedings*, 2014. 3
- [17] Samuli Laine, Janne Hellsten, Tero Karras, Yeongho Seol, Jaakko Lehtinen, and Timo Aila. Modular primitives for high-performance differentiable rendering. *ACM Transactions on Graphics*, 39(6), 2020. 4
- [18] Chen-Hsuan Lin, Jun Gao, Luming Tang, Towaki Takikawa, Xiaohui Zeng, Xun Huang, Karsten Kreis, Sanja Fidler, Ming-Yu Liu, and Tsung-Yi Lin. Magic3d: High-resolution text-to-3d content creation. In *Proceedings of the IEEE/CVF Conference on Computer Vision and Pattern Recognition*, pages 300–309, 2023. 1
- [19] Yuxin Liu, Minshan Xie, Hanyuan Liu, and Tien-Tsin Wong. Text-guided texturing by synchronized multi-view diffusion. In *SIGGRAPH Asia 2024 Conference Papers*, pages 1–11, 2024. 2, 5
- [20] Yufei Liu, Junwei Zhu, Junshu Tang, Shijie Zhang, Jiangning Zhang, Weijian Cao, Chengjie Wang, Yunsheng Wu, and Dongjin Huang. Texdreamer: Towards zero-shot high-fidelity 3d human texture generation. In *European Conference on Computer Vision*, pages 184–202. Springer, 2024. 2
- [21] Gal Metzger, Elad Richardson, Or Patashnik, Raja Giryes, and Daniel Cohen-Or. Latent-nerf for shape-guided generation of 3d shapes and textures. In *Proceedings of the IEEE/CVF Conference on Computer Vision and Pattern Recognition*, pages 12663–12673, 2023. 1, 2
- [22] Oscar Michel, Roi Bar-On, Richard Liu, Sagie Benaim, and Rana Hanocka. Text2mesh: Text-driven neural stylization for meshes. In *Proceedings of the IEEE/CVF Conference*

- on *Computer Vision and Pattern Recognition*, pages 13492–13502, 2022. [2](#)
- [23] Ben Mildenhall, Pratul P Srinivasan, Matthew Tancik, Jonathan T Barron, Ravi Ramamoorthi, and Ren Ng. Nerf: Representing scenes as neural radiance fields for view synthesis. *Communications of the ACM*, 65(1):99–106, 2021. [1](#)
- [24] Nasir Mohammad Khalid, Tianhao Xie, Eugene Belilovsky, and Tiberiu Popa. Clip-mesh: Generating textured meshes from text using pretrained image-text models. In *SIGGRAPH Asia 2022 conference papers*, pages 1–8, 2022. [2](#)
- [25] Jacob Munkberg, Jon Hasselgren, Tianchang Shen, Jun Gao, Wenzheng Chen, Alex Evans, Thomas Müller, and Sanja Fidler. Extracting Triangular 3D Models, Materials, and Lighting From Images. In *Proceedings of the IEEE/CVF Conference on Computer Vision and Pattern Recognition (CVPR)*, pages 8280–8290, 2022. [4](#)
- [26] Michael Oechsle, Lars Mescheder, Michael Niemeyer, Thilo Strauss, and Andreas Geiger. Texture fields: Learning texture representations in function space. In *Proceedings of the IEEE/CVF International Conference on Computer Vision*, pages 4531–4540, 2019. [2](#)
- [27] Ben Poole, Ajay Jain, Jonathan T Barron, and Ben Mildenhall. Dreamfusion: Text-to-3d using 2d diffusion. *arXiv preprint arXiv:2209.14988*, 2022. [1](#), [2](#), [3](#)
- [28] Alec Radford, Jong Wook Kim, Chris Hallacy, Aditya Ramesh, Gabriel Goh, Sandhini Agarwal, Girish Sastry, Amanda Askell, Pamela Mishkin, Jack Clark, et al. Learning transferable visual models from natural language supervision. In *International conference on machine learning*, pages 8748–8763. PMLR, 2021. [2](#)
- [29] Elad Richardson, Gal Metzger, Yuval Alaluf, Raja Giryes, and Daniel Cohen-Or. Texture: Text-guided texturing of 3d shapes. In *ACM SIGGRAPH 2023 conference proceedings*, pages 1–11, 2023. [2](#)
- [30] Robin Rombach, Andreas Blattmann, Dominik Lorenz, Patrick Esser, and Björn Ommer. High-resolution image synthesis with latent diffusion models. In *Proceedings of the IEEE/CVF conference on computer vision and pattern recognition*, pages 10684–10695, 2022. [1](#), [2](#)
- [31] Chitwan Saharia, William Chan, Saurabh Saxena, Lala Li, Jay Whang, Emily L Denton, Kamyar Ghasemipour, Raphael Gontijo Lopes, Burcu Karagol Ayan, Tim Salimans, et al. Photorealistic text-to-image diffusion models with deep language understanding. *Advances in neural information processing systems*, 35:36479–36494, 2022. [1](#), [2](#)
- [32] Yichun Shi, Peng Wang, Jianglong Ye, Mai Long, Kejie Li, and Xiao Yang. Mvdream: Multi-view diffusion for 3d generation. *arXiv preprint arXiv:2308.16512*, 2023. [2](#)
- [33] Alex Shonenkov, Misha Konstantinov, Daria Bakshandaeva, Christoph Schuhmann, Ksenia Ivanova, and Nadiia Klokova. Deepfloyd-iff. *Hugging Face*, 2023. [5](#)
- [34] Yawar Siddiqui, Justus Thies, Fangchang Ma, Qi Shan, Matthias Nießner, and Angela Dai. Texturify: Generating textures on 3d shape surfaces. In *European Conference on Computer Vision*, pages 72–88. Springer, 2022. [2](#)
- [35] Dmitry Ulyanov, Andrea Vedaldi, and Victor Lempitsky. Deep image prior. In *Proceedings of the IEEE conference on computer vision and pattern recognition*, pages 9446–9454, 2018. [5](#), [8](#)
- [36] Kim Youwang, Tae-Hyun Oh, and Gerard Pons-Moll. Paint-it: Text-to-texture synthesis via deep convolutional texture map optimization and physically-based rendering. In *Proceedings of the IEEE/CVF Conference on Computer Vision and Pattern Recognition*, pages 4347–4356, 2024. [1](#), [2](#), [5](#)
- [37] Rui Yu, Yue Dong, Pieter Peers, and Xin Tong. Learning texture generators for 3d shape collections from internet photo sets. In *British Machine Vision Conference*, 2021. [2](#)
- [38] Xianfang Zeng, Xin Chen, Zhongqi Qi, Wen Liu, Zibo Zhao, Zhibin Wang, Bin Fu, Yong Liu, and Gang Yu. Paint3d: Paint anything 3d with lighting-less texture diffusion models. In *Proceedings of the IEEE/CVF Conference on Computer Vision and Pattern Recognition*, pages 4252–4262, 2024. [2](#)

A. Evaluation Protocol Details

A.1. Blender parameters

We render images using *Blender 3.3.21* with the *Cycles* rendering engine. Eval camera positions are taken from a sphere with a radius of 1.4, where the spherical coordinates φ (azimuth angle) and θ (polar angle) are derived from the setup described in Text2Tex. The HDRI light map from [polyhaven](#) used in our experiments is visualized in Figure 7(a); we set the environment map strength to 0.7.

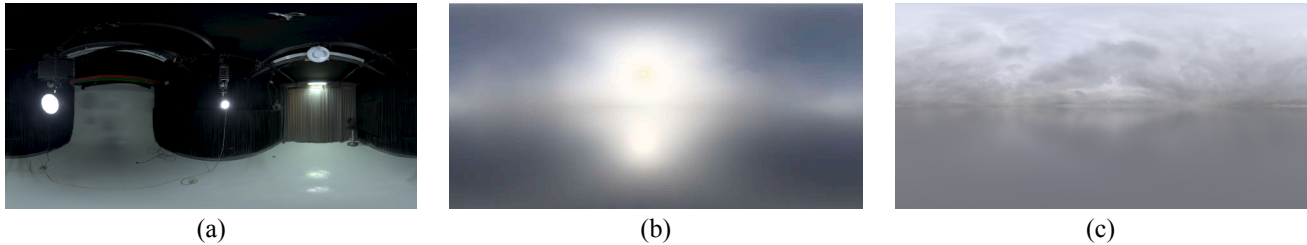


Figure 7. Used HDRI light maps: (a) for evaluation; (b) for our pipeline; (c) for Paint-it.

A.2. Details of User Study

Every assessor was asked to evaluate the setup shown in Figure 8.

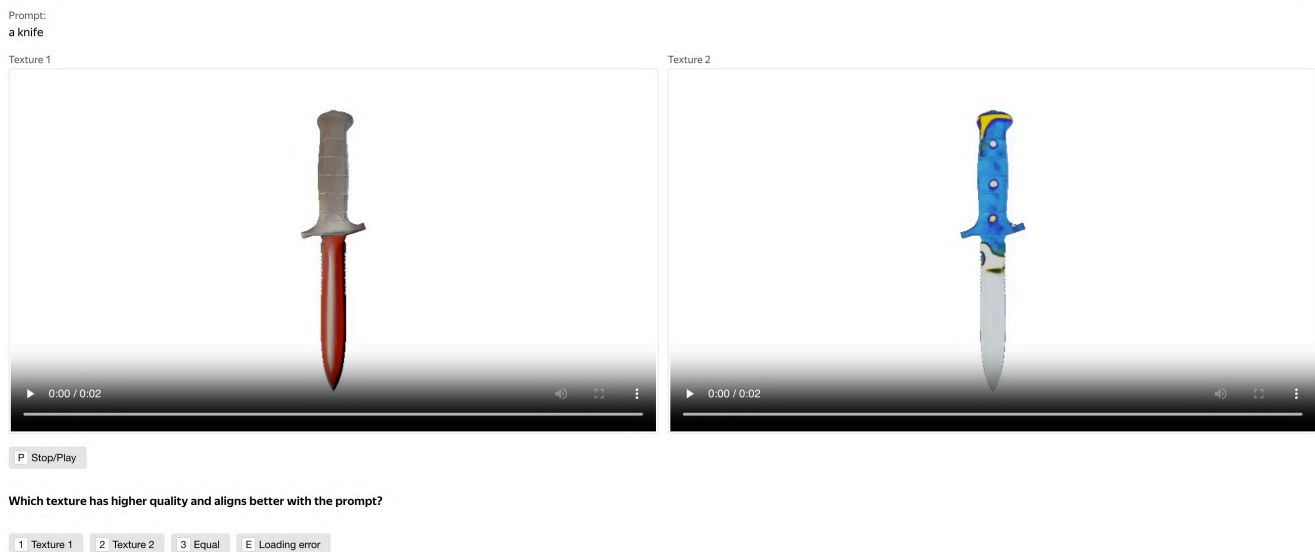


Figure 8. Assessor’s evaluation setup. Professional assessors were tasked with evaluating the quality of the generated textures and selecting the texture that best aligned with the suggested prompt. To ensure unbiased evaluations, the order of the methods was randomly shuffled for each setup.

B. Environment lights

For our texture generation setup, we utilize the HDRI light map visualized in Figure 7(b). In contrast, the Paint-it HDRI light map, shown in Figure 7(c), represents an alternative lighting configuration. All the HDRI light maps used in this work are publicly available for download from [polyhaven](#).

C. Texture Synthesis Results in Varying Setups

In this section, we present textures obtained with different diffusion model combinations to illustrate the impact of model size and the role of the super-resolution module. The results are shown in Figure 9. We also provide additional examples comparing our method with the baselines in Figure 10. Finally, Figure 11 shows a textured model after the first and the second stage of using our cascaded pixel diffusion, compared to the noisy output of latent diffusion.



Figure 9. Textures obtained with middle (M) and extra-large (XL) diffusion models along with their versions improved with large (L) super-resolution model on the second stage.

D. High frequency study in DIP

Our investigation into integrating Deep Image Prior (DIP) with our framework reveals certain limitations that affect its practical utility in texture synthesis. Despite being computationally more expensive, our experiments suggest that DIP may not provide sufficient benefits to justify its implementation costs.

As shown in Figure 12, spectral analysis conducted on the Objaverse dataset [11] demonstrates why the parameterization of DIP performs poorly compared to our standard explicit approach. The spectral plot (Figure 12(a)) reveals DIP’s significant deficiency in high-frequency components, visually translating to outputs with noticeably less textural detail and surface variation. To further illustrate this effect, we provide additional examples in Figure 12(b) using two cow prompts, which clearly demonstrate the degradation of the detail in the generation based on DIP.

This limitation in creating detailed textures further validates our choice of explicit parameterization, which achieves better visual quality and quantitative metrics with less computational cost.

E. Visualization of PBR Texture Maps

Even though physically based texture improve the overall results, our method occasionally struggles to fully disentangle the lighting effects. We visualize a few examples in Figure 14. For instance, consider partially baked highlights on the coffee maker or the suitcase.

Figure 13 further evaluates prompt-conditioned control on a fixed mesh: we change only the material description and generate the corresponding PBR maps. The generator consistently shifts the distributions of metalness, roughness, and normal amplitude in a physically meaningful way, indicating that it learns material semantics rather than merely recoloring the surface. Metals remain the most sensitive case, where map statistics can still correlate with lighting; we attribute this to limited light map diversity and leave stronger lighting disentanglement for future work.

Objaverse mesh with input text		Text2Tex	SyncMVD	Paint-It	FlashTex	CasTex (ours)
"dog"						
"boat"						
"baseball glove"						
"cowboy hat"						
"pigeon"						
"banjo"						
"microscope"						
"watermelon"						
"binoculars"						
Texture type / Relightable?		RGB / ❌	RGB / ❌	PBR / ✅	PBR / ✅	PBR / ✅

Figure 10. Additional samples from the Objaverse dataset.

Prompt: “alarm clock”

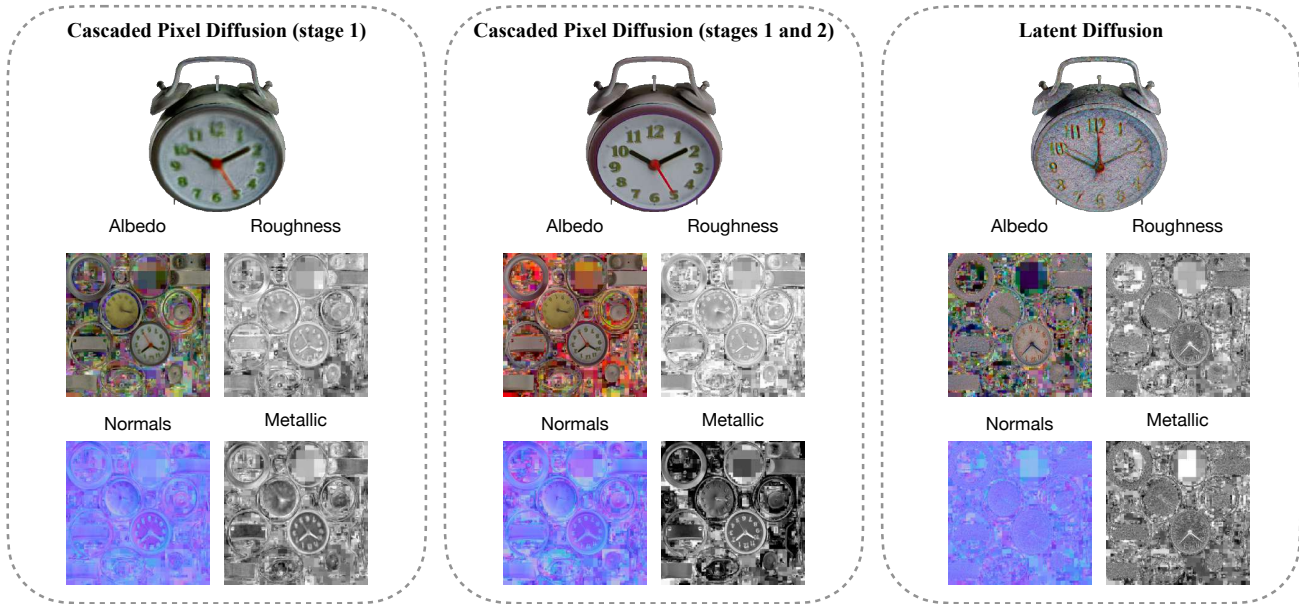


Figure 11. Textured model after the first and the second stage of our cascaded pixel diffusion, compared to the noisy result from latent diffusion.

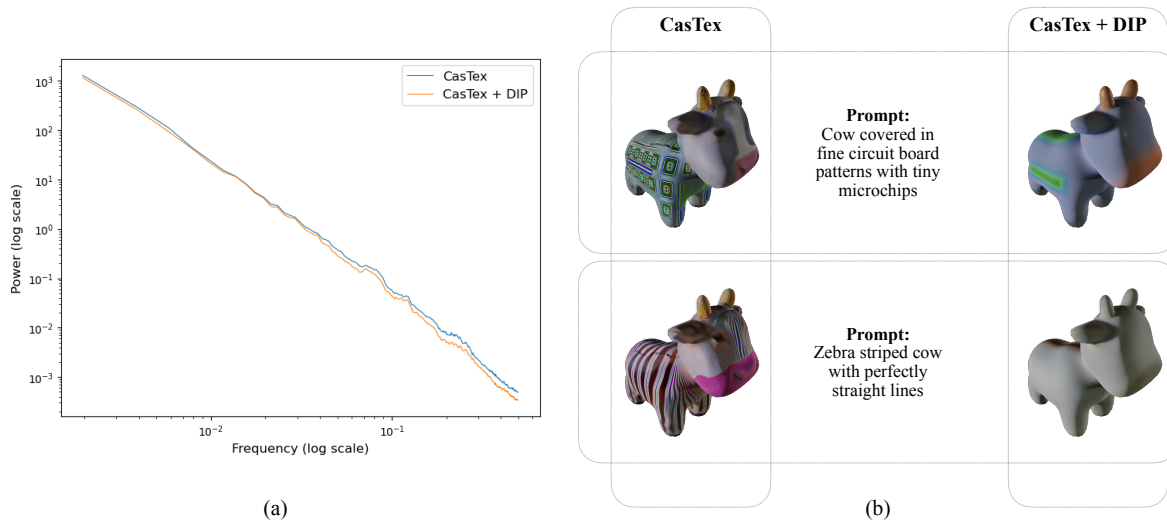


Figure 12. Spectral and visual comparison of texture generation approaches. (a) Power spectrum analysis (log scale) computed on the Objaverse subset, showing CasTex + DIP’s reduced power in high-frequency components compared to standard CasTex . (b) Additional examples showing texture generation results for two test prompts. CasTex produces rich, detailed textures while CasTex + DIP generates simplified outputs lacking fine-grained details, directly corresponding to its high-frequency limitations observed in the spectral analysis.

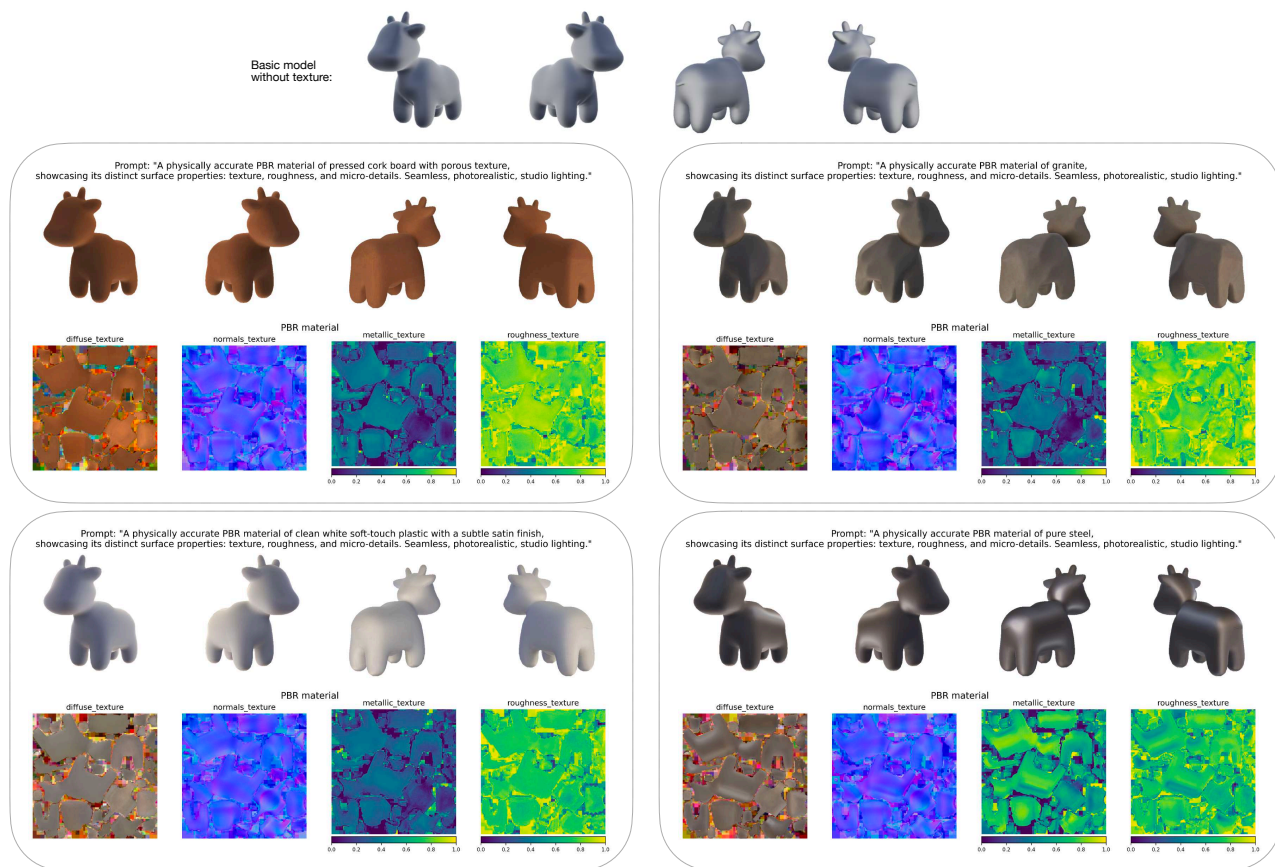


Figure 13. Prompt-conditioned PBR textures demonstrating prompt-level control over material properties. *Top-left (cork)*: high roughness variation, porous normal detail, near-zero metalness. *Top-right (granite)*: stone-like appearance from speckled albedo and fine normals; non-metallic, mid-high roughness. *Bottom-left (soft-touch plastic)*: uniform albedo, near-zero metalness, satin roughness, low-amplitude normals. *Bottom-right (steel)*: high metalness and lower roughness; residual noise and partially baked highlights remain—likely due to limited environment-lighting variation; improving metal disentanglement is future work.

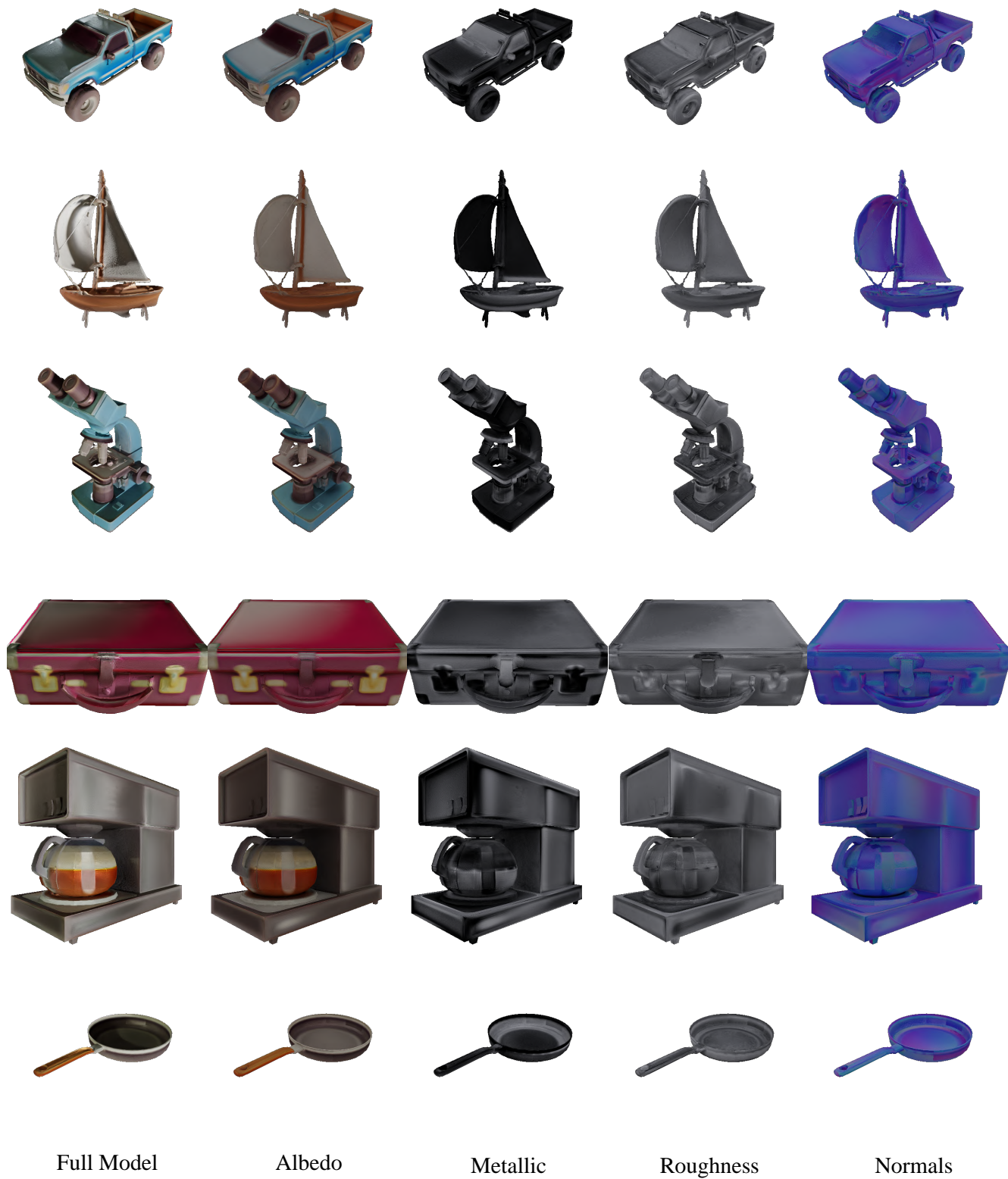


Figure 14. Visualization of the PBR textures. Lighter colors indicate higher metallic and roughness values for the corresponding texture components.